Volume 2, No. 2 May 2015 ISSN: 2148-3981

Ankara University
Institute of Nuclear Sciences

Journal of Nuclear Sciences

Owner on behalf of Institute of Nuclear Sciences,
Ankara University,
Director

Niyazi MERİÇ, Ph.D.

http://jns.ankara.edu.tr

Hosted by Ankara University

Journal of Nuclear Sciences

ISSN: 2147-7736

Journal home page: http://jns.ankara.edu.tr/

DOI: 10.1501/nuclear_0000000011

Synthesis and characterization of new phosphor based $MTiO_3$

N. Kayacı[1], S. Dayan[1], A. K. Küçük[1], N. Kalaycıoğlu Özpozan[*1],
E. Öztürk[2], E. Karacaoğlu[2]

[1]*Department of Chemistry, Faculty of Science, Erciyes University, 38039 Kayseri, Turkey*
[2]*Materials Science and Engineering, Faculty of Engineering, Karamaoğlu Mehmetbey University, 70200, Karaman, Turkey*

Received 13.11.2014; accepted 02.04.2015

ABSTRACT

In this study, new titanate phosphors were synthesized. The Dy^{3+}, Eu^{3+}, Ho^{3+} rare-earth ions were used as dopants to $CaTiO_3$, $SrTiO_3$, and $BaTiO_3$ host crystals. The optimization of reaction conditions were carried out by thermogravimetry (TG) and differential thermal analysis (DTA) methods. The mixtures to achieve a solid state reaction were heated in porcelain crucibles for preheating process at 600 °C and 800 °C and final heating process at 1000 °C for 16 hours in the open atmosphere. The reaction products were characterized by X-ray powder diffractions (XRD). Surface investigations and elemental analysis were determined by using SEM-EDX instrument.
Photoluminescence spectrophotometer (PL) was used for the observation of the excitation and emission spectra.

Keywords: Perovskite, Luminescence, Phosphors, Solid state synthesis techniques, XRD

1. Introduction

Over the last several decades, a formula of perovskites, ABO_3 has attracted broad interest due to their piezoelectricity, ferroelectricity, colossal magneto resistivity, and photoluminescence [1–4]. Perovskite and ilmenite oxides which are the structure of ABO_3, represent a prominent of advanced compounds involved in many areas of science and technology [5–7]. Several titanates are also known to be promising host matrices. The PL investigations of barium titanate have been extensively discussed by Moreira et al [8]. In addition, the PL of several other titanate systems such as gadolinium titanate, zirconium titanate, strontium titanate, lead titanate and calcium titanate, and magnesium titanate are available in the literature [9–12]. The interest in the PL of these titanate based systems is due to the fact that the TiO_2 group in these matrices has a relatively wide band gap and high refractive index, which results in intense luminescence; for this reason, these titanate-based compounds can find potential applications in optoelectronic devices [13]. Moreover, the TiO_2 structure itself possesses good mechanical strength and thus can withstand corrosive environments. The chromaticity of these titanate systems can be controlled to a large extent by suitable doping with a 3d or 4f system and by controlling the various synthesis parameters [14].

In this study, $CaTiO_3$, $CaTiO_3$: Eu^{3+} (1% mol), Dy^{3+} (1% mol), $SrTiO_3$, $SrTiO_3$: Eu^{3+} (1% mol), Dy^{3+} (1% mol), $SrTiO_3$: Ho^{3+} (1% mol), Dy^{3+} (1% mol), $BaTiO_3$, $BaTiO_3$: Dy^{3+} (1% mol), Ho^{3+} (1% mol), $BaTiO_3$: Dy^{3+} (1% mol), Eu^{3+} (1% mol) were synthesized by solid-state reaction. Their thermal behaviors, crystal structures, photoluminescence properties and structural features were investigated.

2. Experimental

Rare-earth ions containing calcium titanate, strontium titanate and barium titanate were prepared by heating a mixture with a ratio of 1 mol of calcium nitrate ($Ca(NO_3)_2$) (A.R.) or strontium nitrate ($Sr(NO_3)_2$) (A.R.) or barium nitrate $Ba(NO_3)_2$, 1 mol of tetra-n-butyl titanate ($Ti(OC_4H_9)_4$) (A.R.) and 0.01 mol of rare-earth nitrate of 99.99 % purity in an air atmosphere. During the grinding process with agate mortar (about 2 hours), the pasty mixtures became powder form due to alcohol moving away from $Ti(OC_4H_9)_4$.
Firstly, TG/DTA system (Perkin Elmer Diamond, USA) was used to determine the reaction conditions in the temperature range 50–1200 °C under an inert N_2 atmosphere with a heating rate 10 °C/min.
After TG/DTA analysis, according to thermal analysis data, the mixtures were pre-heated in controlled oven at 600 °C for 2 h and 800 °C for 2 h and then pre-heated mixtures were heated at 1000 °C

*Corresponding author.
E-mail address: nozpozan@erciyes.edu.tr (N. Kalaycıoğlu Özpozan)
Journal of Nuclear Sciences, Vol. 2, No.2, May 2015, 31-47

ISSN: 2147-7736

for 16 h. After heating procedure, $CaTiO_3$: RE (RE= Eu^{3+}/Dy^{3+}), $SrTiO_3$:RE (RE=Eu^{3+}/Dy^{3+} and Ho^{3+}/Dy^{3+}) and $BaTiO_3$:RE (RE=Dy^{3+}/Ho^{3+} and Dy^{3+}/Eu^{3+}) were synthesized by solid state reaction.
Structural characterization was analyzed by X-ray diffraction (XRD; Bruker AXS D8) spectra with CuKα line of 1.5406 Å. Scanning electron microscopy (SEM) images and EDX analysis were taken with a LEO 440 model scanning electron microscope using an accelerating voltage of 20 kV.
Excitation and emission spectra of the phosphors were investigated by Varian Cary Eclipse luminescence spectrophotometer with xenon lamp and a Perkin Elmer LS 45 model luminescence spectrophotometer with xenon lamp.

3. Results and Discussion

3.1 Characterization of samples

Thermal behaviors of mixtures were analyzed using TG/DTG/DTA system. The TG/DTG/DTA results for the samples are shown in Fig. 1.
The $Ca(NO_3)_2$-$Ti(OC_4H_9)_x$ mixture gives 3 endothermic peaks between 50 ºC and 480 ºC. The peak which indicated a mass loss in the ratio of 22% in TG corresponds to butyl alcohol separated from the medium. The main weight loss of 23% observed at 560 ºC indicates decomposition of $Ca(NO_3)_2$ which is transformed into CaO. The weight loss of the mixture continues until 560 ºC to 1200 ºC.
The $Sr(NO_3)_2$-$Ti(OC_4H_9)_x$ mixture gives two endothermic peaks between 50 ºC and 490 ºC. The peak which indicated a mass loss in the ratio of 24% in TG corresponds to butyl alcohol separated from the medium. The main weight loss of 23% observed at 598 ºC indicates decomposition of $Ca(NO_3)_2$ which is transformed into SrO.
The $Ba(NO_3)_2$-$Ti(OC_4H_9)_x$ mixture gives one endothermic peak between 50 ºC and 500 ºC. The peak which indicated a mass loss in the ratio of 22% in TG corresponds to butyl alcohol separated from the medium. The main weight loss of 20% observed at 597 ºC indicates decomposition of $Ca(NO_3)_2$ which is transformed into SrO. 2% weight loss was observed after 600 degrees of the resulting peak, corresponding to the sublimation material.
The TG/DTA curves of $CaTiO_3$ and $CaTiO_3$: Eu^{3+} (1% mol), Dy^{3+} (1% mol) synthesized at 1000 ºC are shown in Fig.2. $Ca(NO_3)_2$ has lost 4% mass at 47-1240 ºC. According to DTA, any phase change was not identified at the temperature range 47 -1240 ºC.
The TG/DTA curves of $SrTiO_3$, $SrTiO_3$: Eu^{3+}(1% mol), Dy^{3+} (1% mol) and $SrTiO_3$: Ho^{3+} (1% mol), Dy^{3+} (1% mol) synthesized at 1000 ºC are shown in Fig. 3. Any losing mass or phase change was not determined at the temperature range 48 ºC - 1243 ºC.
The TG/DTA curves of $BaTiO_3$, $BaTiO_3$: Dy^{3+} (1% mol), Ho^{3+} (1% mol) and $BaTiO_3$: Dy^{3+} (1% mol), Eu^{3+} (1% mol) synthesized at 1000 ºC are shown in Fig. 4. The samples did not lose mass and the phase change was not identified at the temperature range 40 ºC - 1450 ºC.

3.2 Phase formation analysis

The $CaTiO_3$ and $CaTiO_3$: Eu^{3+} (1% mol), Dy^{3+} (1% mol) were applied pre-heat treatment at 600 ºC for 2 h and at 800 ºC and then solid state reaction was performed at 1000 ºC for 16 h. At the end of heat treatment, samples' color changed to white color. XRD patterns of $CaTiO_3$ and $CaTiO_3$: Eu^{3+}(1% mol), Dy^{3+}(1%mol) calcined at 1000 ˚C are shown in Fig.5. The crystal systems of samples were indexed in an orthorhombic crystal system. Unit cell parameters of samples are listed in Table 1 and powder XRD pattern data of $CaTiO_3$ and $CaTiO_3$: Eu^{3+} (1% mol), Dy^{3+} (1% mol) are listed in Table 2, and Table 3. These values show very good agreement with reference value of $CaTiO_3$. $CaTiO_3$ has an orthorhombic crystal system with a = 763.9 pm, b = 544.0 pm, c = 538.0 pm; V= 224x10^6 pm^3 [15].
For the $SrTiO_3$, $SrTiO_3$: Eu^{3+} (1% mol), Dy^{3+} (1% mol), $SrTiO_3$: Ho^{3+}(1% mol), Dy^{3+}(1% mol) and $BaTiO_3$: Dy^{3+} (1% mol), Ho^{3+}(1% mol), $BaTiO_3$: Dy^{3+} (1% mol) , Eu^{3+} (1% mol) , pre-heat treatment at 600 ºC and 800 ºC for 2 h was applied. Then solid state reaction was performed at 1000 ºC for 16 h. At the end of heat treatment, samples' color changed to white color. XRD patterns of $SrTiO_3$, $SrTiO_3$: Eu^{3+} (1% mol), Dy^{3+} (1% mol), $SrTiO_3$: Ho^{3+} (1% mol), Dy^{3+} (1% mol) are shown in Fig. 6. Cubic unit cell parameters of samples are listed in Table 5 and powder XRD pattern data of $SrTiO_3$, $SrTiO_3$: Eu^{3+} (1% mol), Dy^{3+} (1% mol) and $SrTiO_3$: Ho^{3+} (1% mol), Dy^{3+} (1% mol) are listed in Table 5-7 respectively. These values show good agreement with reference value of $SrTiO_3$. $SrTiO_3$ has a cubic crystal system with a = 390.50 pm; V= 596x10^5 pm^3 [16]. XRD patterns of $BaTiO_3$: Dy^{3+} (1% mol), Ho^{3+}(1% mol), $BaTiO_3$:Dy^{3+}(1% mol), Eu^{3+}(1% mol) are shown in Fig. 7. Tetragonal unit cell parameters of samples are listed in Table 8 and powder XRD pattern data of $BaTiO_3$, $BaTiO_3$: Dy^{3+} (1% mol), Ho^{3+} (1% mol) and $BaTiO_3$ Dy^{3+} (1% mol), Eu^{3+} (1% mol) are listed in Tables 9-11 respectively. These values show good agreement with reference value of $BaTiO_3$. $BaTiO_3$ has a tetragonal crystal system with a = 399.4 pm, c = 403.3 pm; V= 643x10^5 pm^3 [8].
Heat treatment at 1000 ºC was applied to $CaTiO_3$ and $CaTiO_3$: Eu^{3+}(1% mol), Dy^{3+}(1% mol) were applied before SEM analyses were performed. SEM images of $CaTiO_3$ and $CaTiO_3$:Eu^{3+}(1% mol), Dy^{3+}(1% mol) are shown in Fig. 8.
SEM images of $SrTiO_3$, $SrTiO_3$: Eu^{3+}(1% mol), Dy^{3+} (1% mol) and $SrTiO_3$: Ho^{3+} (1% mol), Dy^{3+} (1%mol) are shown in Fig. 9.

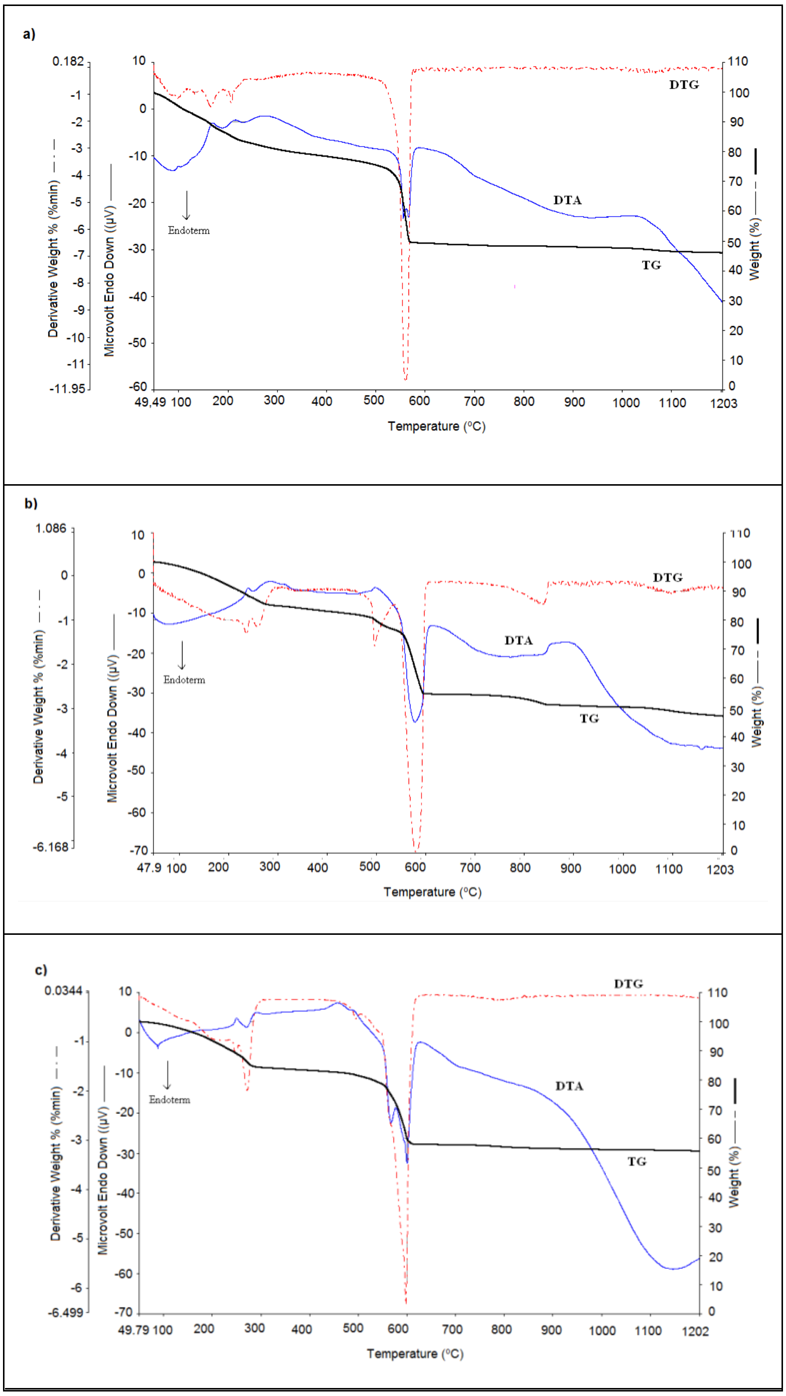

Fig.1. TG/DTG/DTA curves of a) $Ca(NO_3)_2$-$Ti(OC_4H_9)_x$ mixture, b) $Sr(NO_3)_2$-$Ti(OC_4H_9)_x$ mixture and c) $Ba(NO_3)_2$-$Ti(OC_4H_9)_x$ mixture

SEM images of $BaTiO_3$, $BaTiO_3$: Dy^{3+} (1% mol), Ho^{3+} (1% mol) and $SrTiO_3$: Dy^{3+} (1% mol), Eu^{3+} (1% mol) are shown in Fig. 10.

Fig. 11, 12 and 13 show the images and EDX analysis obtained from the SEM measurements of the phosphors calcined at 1000 °C for 2 h by using solid state reactions. The microstructures of the phosphor consisted of regular fine grains with an average size of about150-300 nm. The EDX analysis of the chemical composition of the samples confirms the results of the experimental evidence. EDX analysis results of phosphors are listed in Table 12.

3.3 Luminescence properties

After heated at 1000 °C, excitation and emission luminescence spectra of $CaTiO_3$ doped with Eu^{3+}(1% mol), Dy^{3+}(1% mol) is shown in Fig. 14. The sample is excited at 219 nm and 395 nm. Fewer than 218 and 395 nm excitation wavelength, $CaTiO_3$ doped with Eu^{3+} (1% mol), Dy^{3+} (1% mol) have an emission band at 590 nm. The emission band belongs to $^5D_0 \rightarrow {}^7F_1$ transition of Eu^{3+} ions. Additionally, the sample has yellow color under UV lamp excitation with 366 nm.

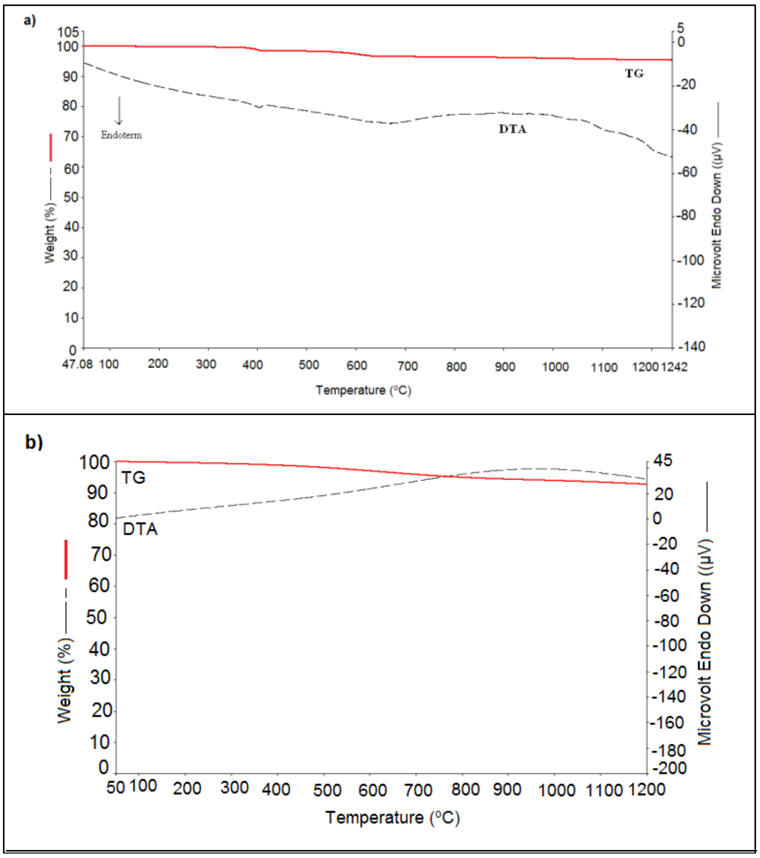

Fig. 2. TG/DTA thermograms of a) $CaTiO_3$ b) $CaTiO_3$: Eu^{3+}(1% mol), Dy^{3+}(1% mol) samples

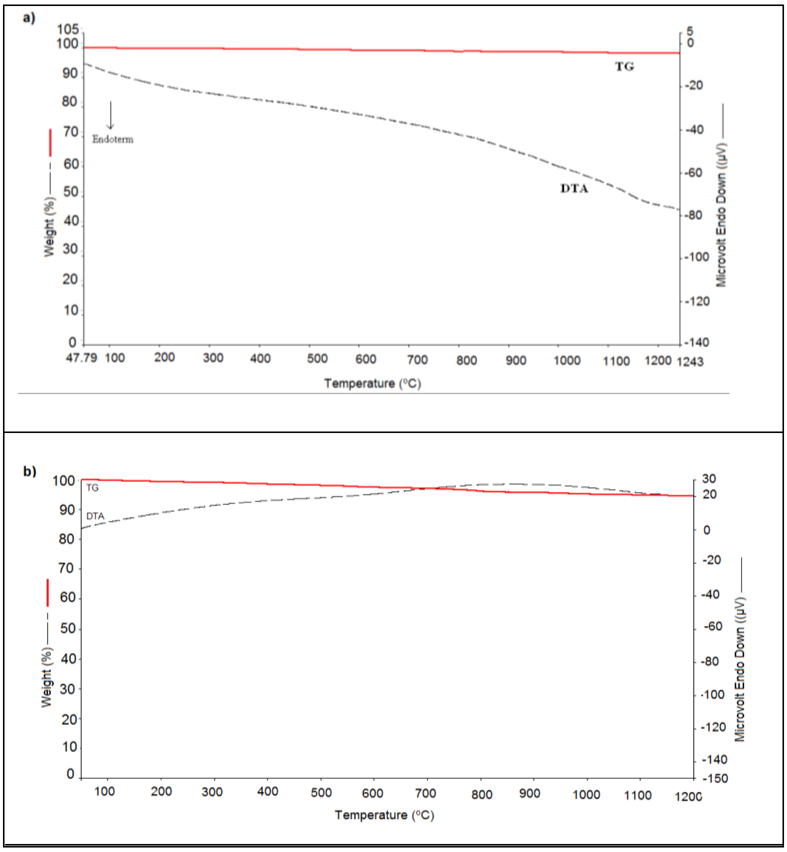

Fig. 3. TG/DTA thermograms of a) $SrTiO_3$ b) $SrTiO_3$: Eu^{3+} (1% mol), Dy^{3+}(1% mol) samples

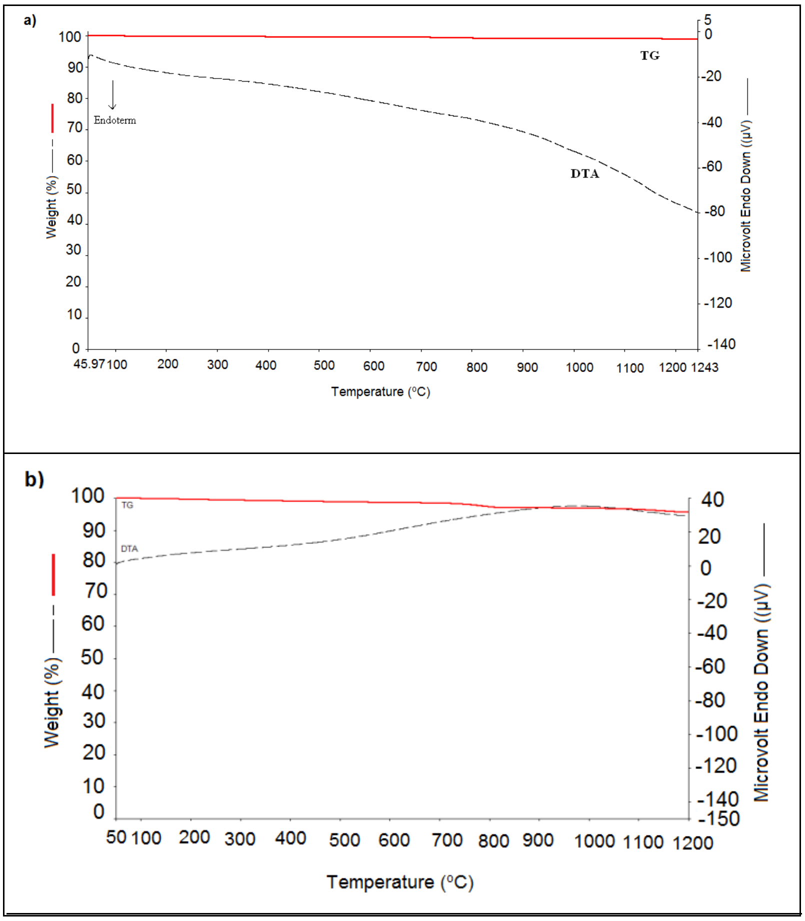

Fig. 4. TG/DTA thermograms of a) $BaTiO_3$ b) $BaTiO_3$: Dy^{3+}(1% mol), Ho^{3+}(1% mol) samples

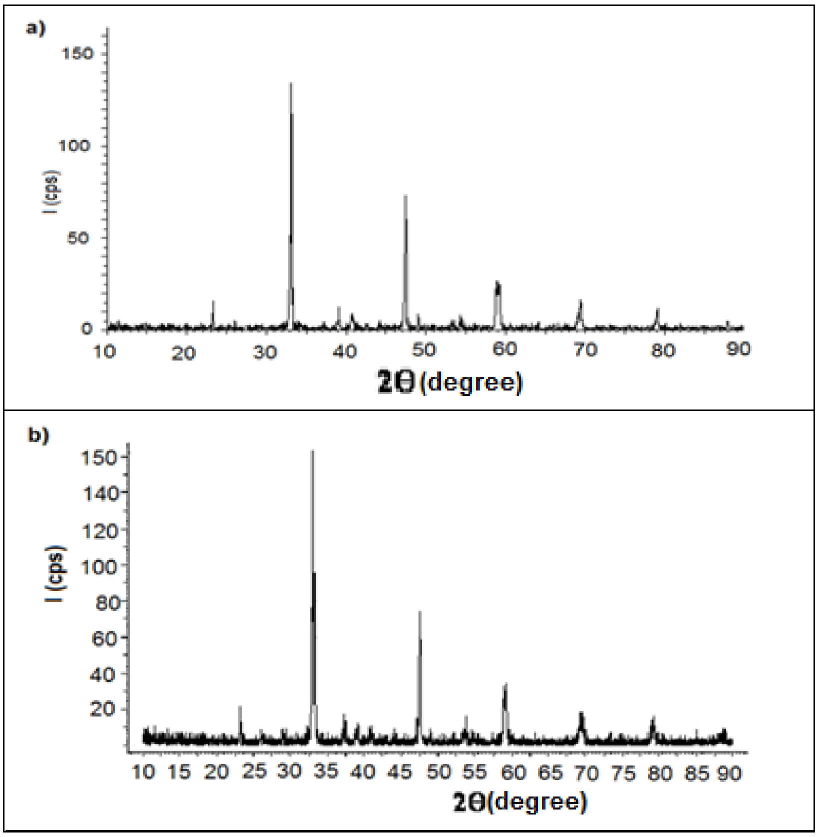

Fig.5. The indexed XRD pattern of a) $CaTiO_3$ and b) $CaTiO_3$: Eu^{3+} (1% mol), Dy^{3+} (1% mol) at 1000 °C

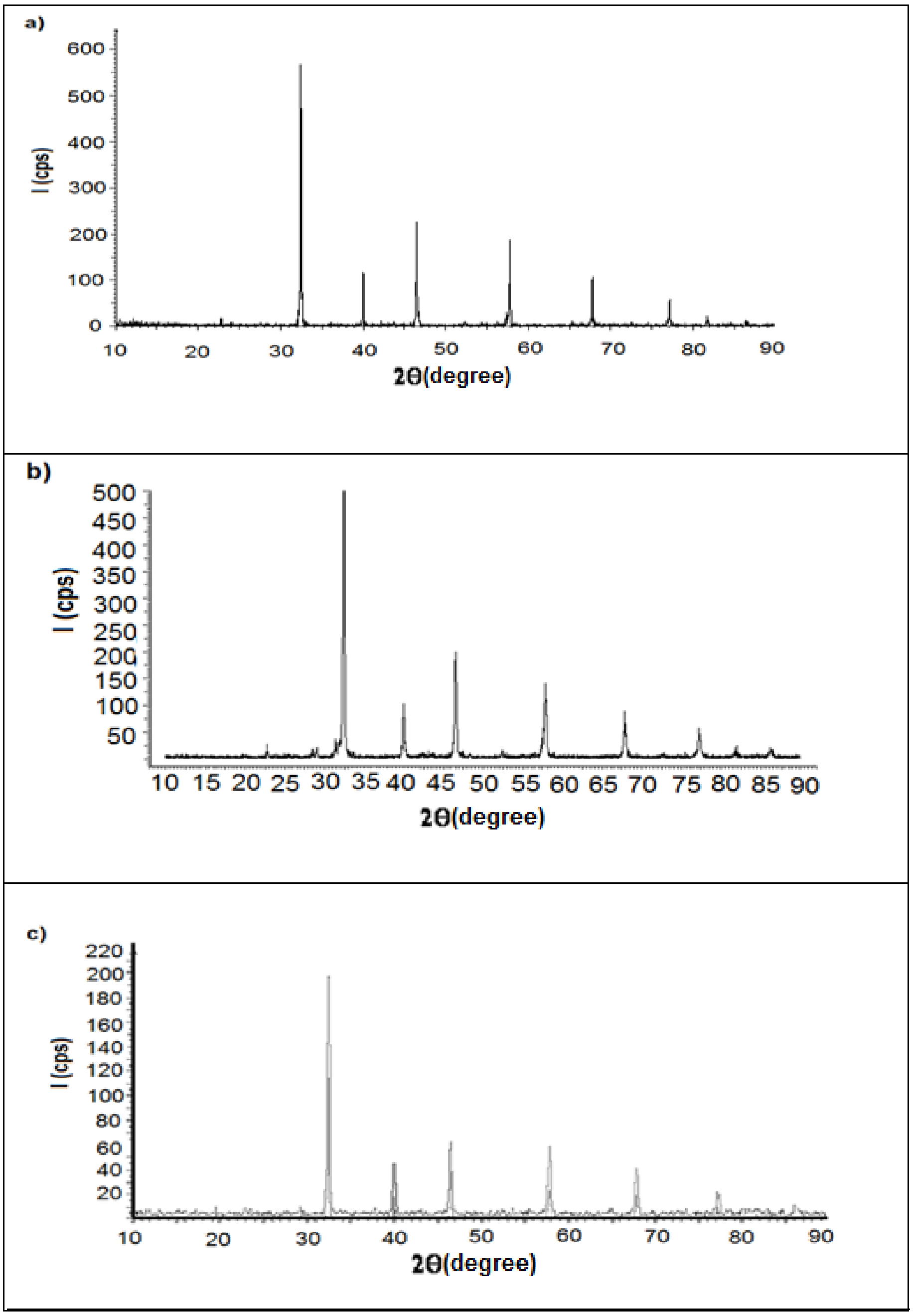

*Fig. 6. The indexed XRD pattern of **a)** $SrTiO_3$, (**b)** $SrTiO_3$: Eu^{3+} (1% mol), Dy^{3+} (1% mol) and **c)** $SrTiO_3$: Ho^{3+} (1% mol), Dy^{3+} (1% mol) at 1000 °C*

Excitation and emission spectra of $SrTiO_3$ doped with Eu^{3+} (1% mol), Dy^{3+} (1% mol) are shown in Fig. 15. The sample is excited at 205 nm and 310 nm. Fewer than 205 and 310 nm excitation wavelength, $SrTiO_3$ doped with Eu^{3+}(1% mol), Dy^{3+}(1% mol) have an emission band at 612 nm. The emission band belongs to $^5D_0 \rightarrow {}^7F_2$ transition of Dy^{3+} ions. Additionally, the sample has yellow color under UV lamp excitation with 366 nm.

Excitation and emission spectra of $BaTiO_3$ doped with Dy^{3+} (1% mol), Ho^{3+}(1% mol) are shown in Fig. 16. The sample is excited at 200 nm and 800 nm. Fewer than 200 nm and 800 nm excitation wavelengths, $SrTiO_3$ doped with Eu^{3+} (1% mol), Dy^{3+}(1% mol) have an emission bands at 546 nm and 584 nm. The emission band belongs to $^4I_{15/2} \rightarrow {}^6H_{15/2}$ transition of Dy^{3+} ions and $^4F_{9/2} \rightarrow {}^6H_{13/2}$ transition of Ho^{3+}. Additionally, the sample has yellow color under UV lamp excitation with 366 nm.

Excitation and emission spectra of $BaTiO_3$ doped with Dy^{3+}(1% mol), Eu^{3+}(1% mol) are shown in Fig.17. The sample is excited at 200 nm and 800 nm. Fewer than 200 and 800 nm excitation wavelengths, $BaTiO_3$ doped with Dy^{3+} (1% mol), Eu^{3+} (1% mol) have an emission bands at 590 nm, 610 nm and 687 nm. The emission bands belong to. $^5D_0 \rightarrow {}^7F_1$, $^5D_0 \rightarrow {}^7F_2$ and $^5D_0 \rightarrow {}^7F_4$ transition of Eu^{3+} ions. There is no band of Dy^{3+} ion. Additionally, the sample has yellow color under UV lamp excitation with 366 nm.

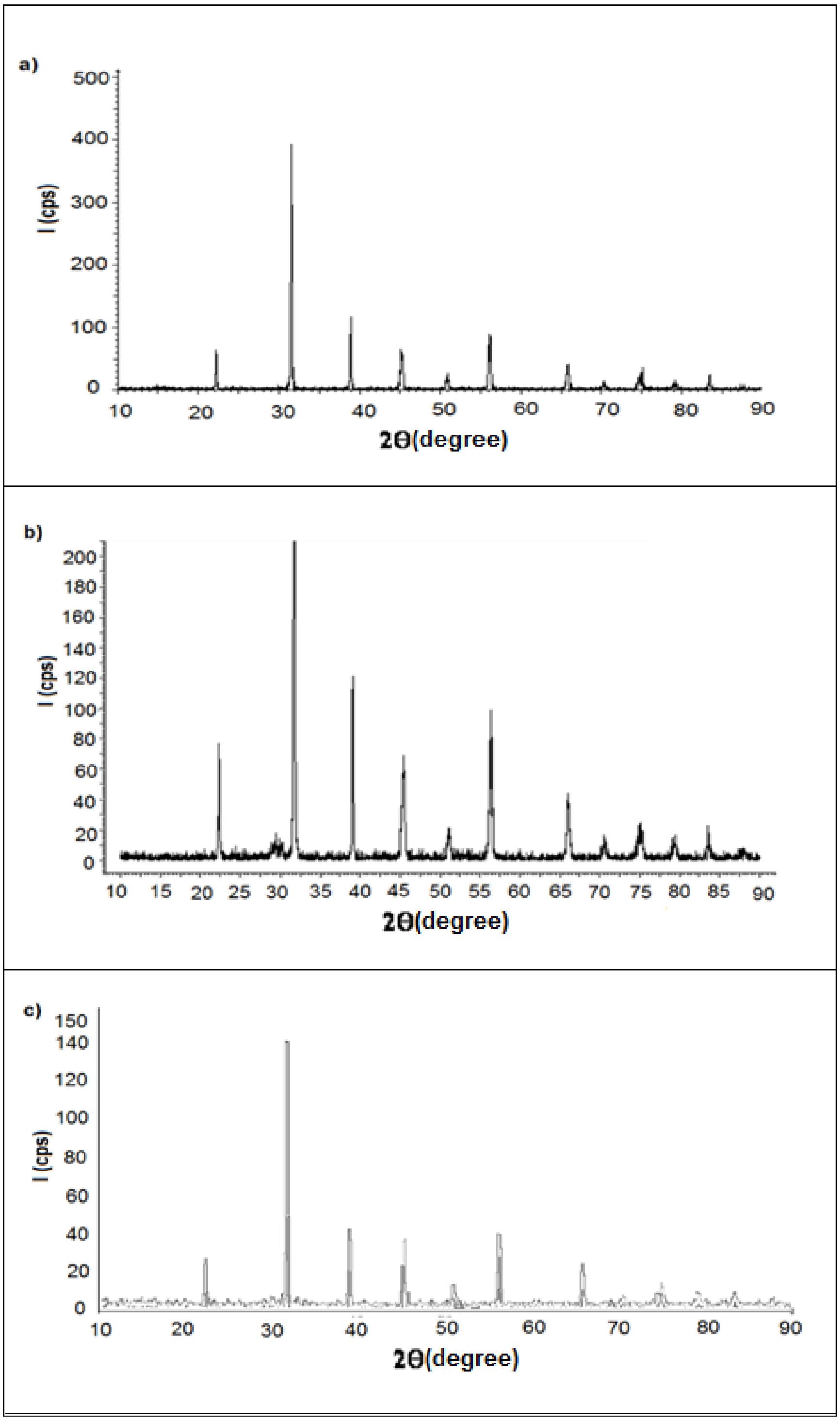

Fig. 7. The indexed XRD pattern of (a) $BaTiO_3$, (b) $BaTiO_3$: Dy^{3+}(1% mol), Ho^{3+}(1% mol) and (c) $BaTiO_3$: Dy^{3+} (1% mol), Eu^{3+}(1% mol) at 1000 °C

Table 1. Unit cell parameters of $CaTiO_3$ and $CaTiO_3$: Eu^{3+}(1% mol), Dy^{3+}(1% mol)

Sample	**a/pm**	**b/pm**	**c/pm**	**V/pm^3**
$CaTiO_3$	763.90	544.00	538.00	224.10^6
$CaTiO_3$: Eu^{3+}(1%) Dy^{3+} (1%)	764.88	543.66	537.10	223.10^6

(a) **(b)**

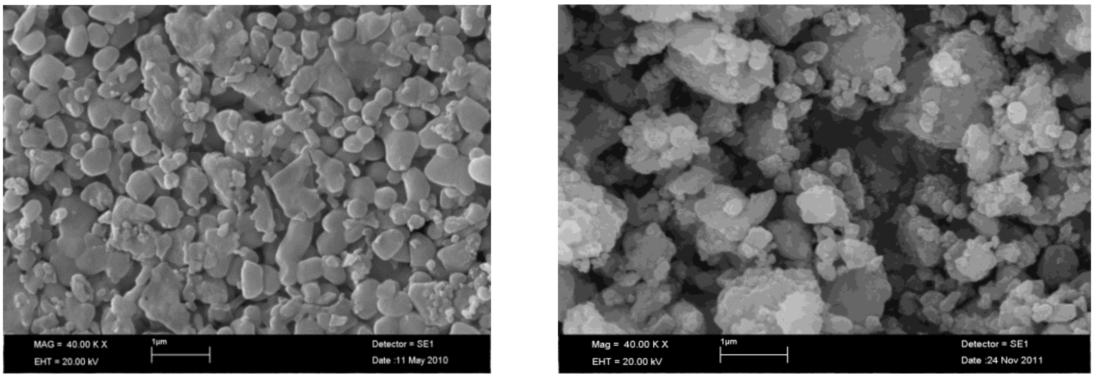

Fig. 8. SEM images of (a) $CaTiO_3$ and (b) $CaTiO_3$: Eu^{3+}(1% mol), Dy^{3+}(1% mol)

(a) **(b)** **(c)**

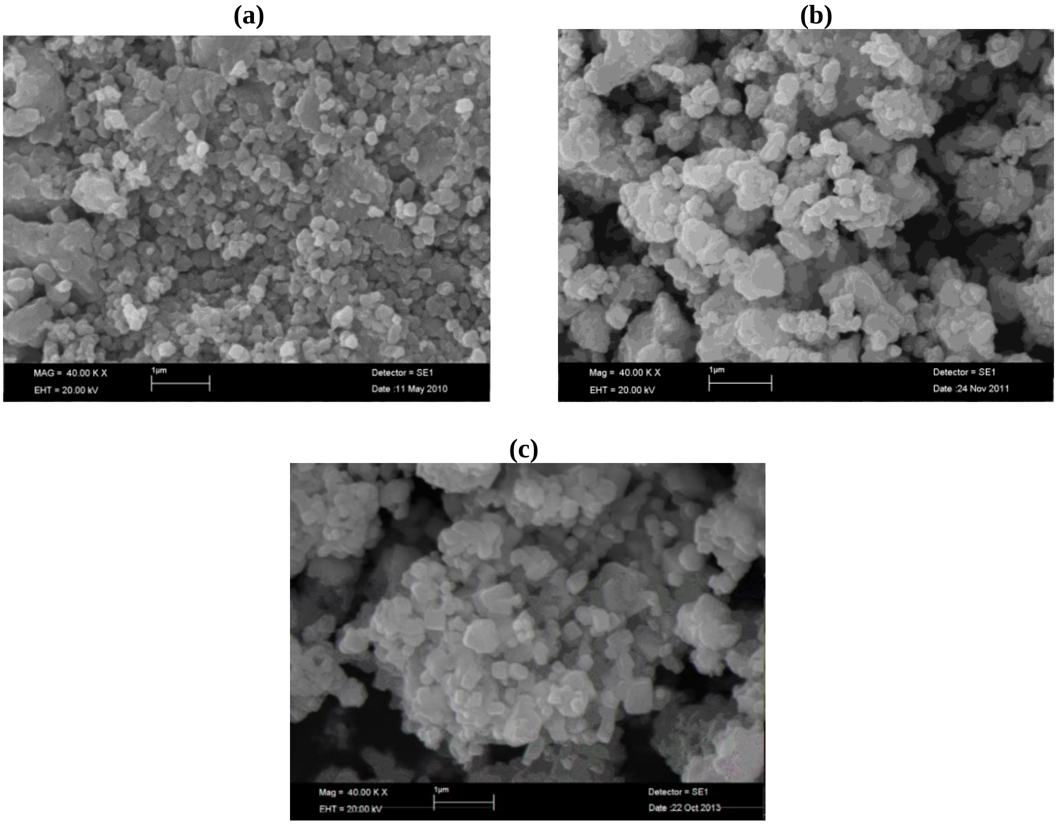

Fig.9. SEM images of (a) $SrTiO_3$, (b) $SrTiO_3$:Eu^{3+}(1% mol), Dy^{3+} (1% mol) and (c) $SrTiO_3$: Ho^{3+}(1% mol), Dy^{3+}(1% mol)

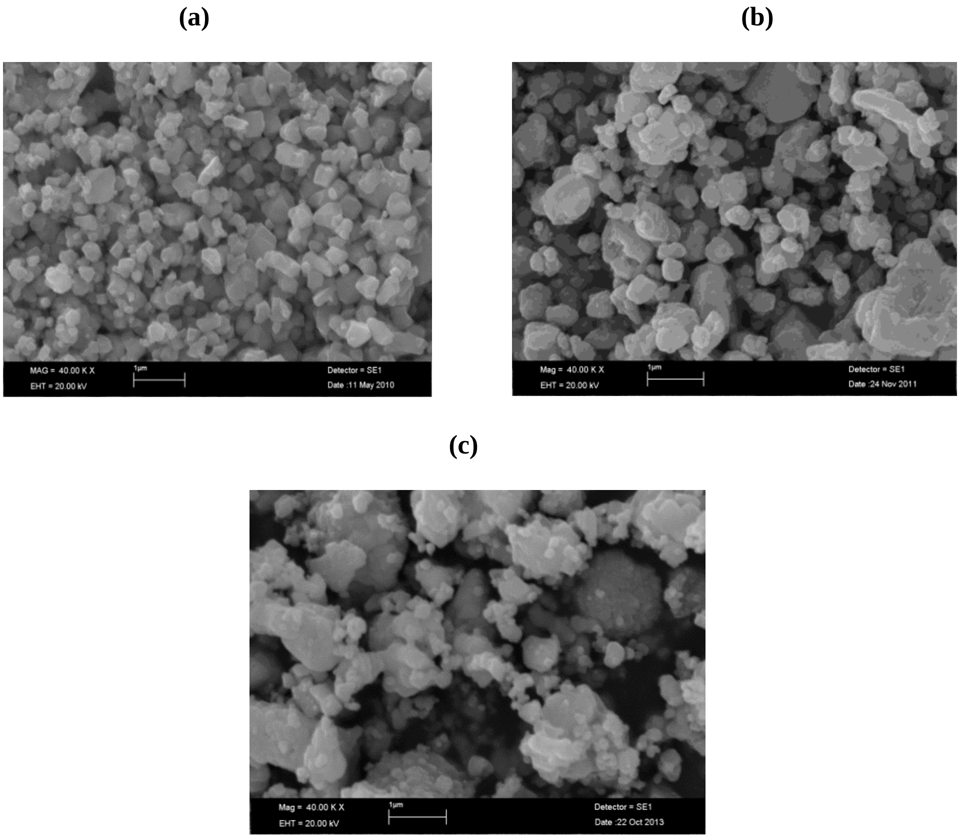

Fig.10. SEM image of (a) $BaTiO_3$, (b) $BaTiO_3$:Dy^{3+} (1% mol), Ho^{3+} (1% mol) and (c) $BaTiO_3$: Dy^{3+}(1% mol), Eu^{3+}(1% mol)

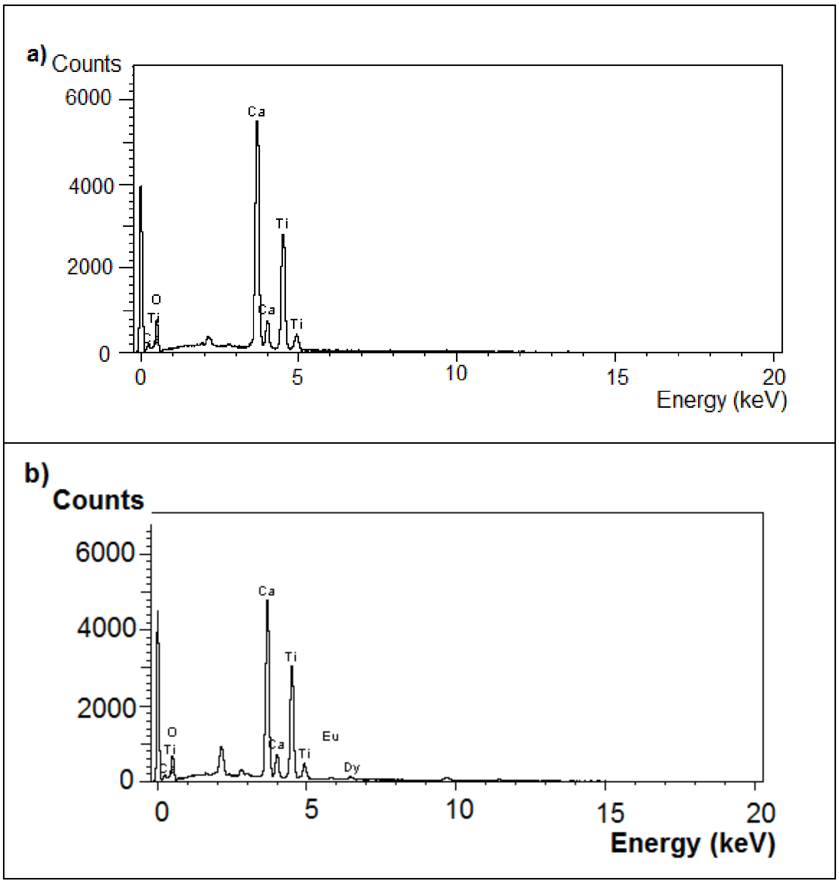

Fig.11. EDX analysis of (a) $CaTiO_3$ and (b) $CaTiO_3$: Eu^{3+}(1% mol), Dy^{3+}(1% mol) samples

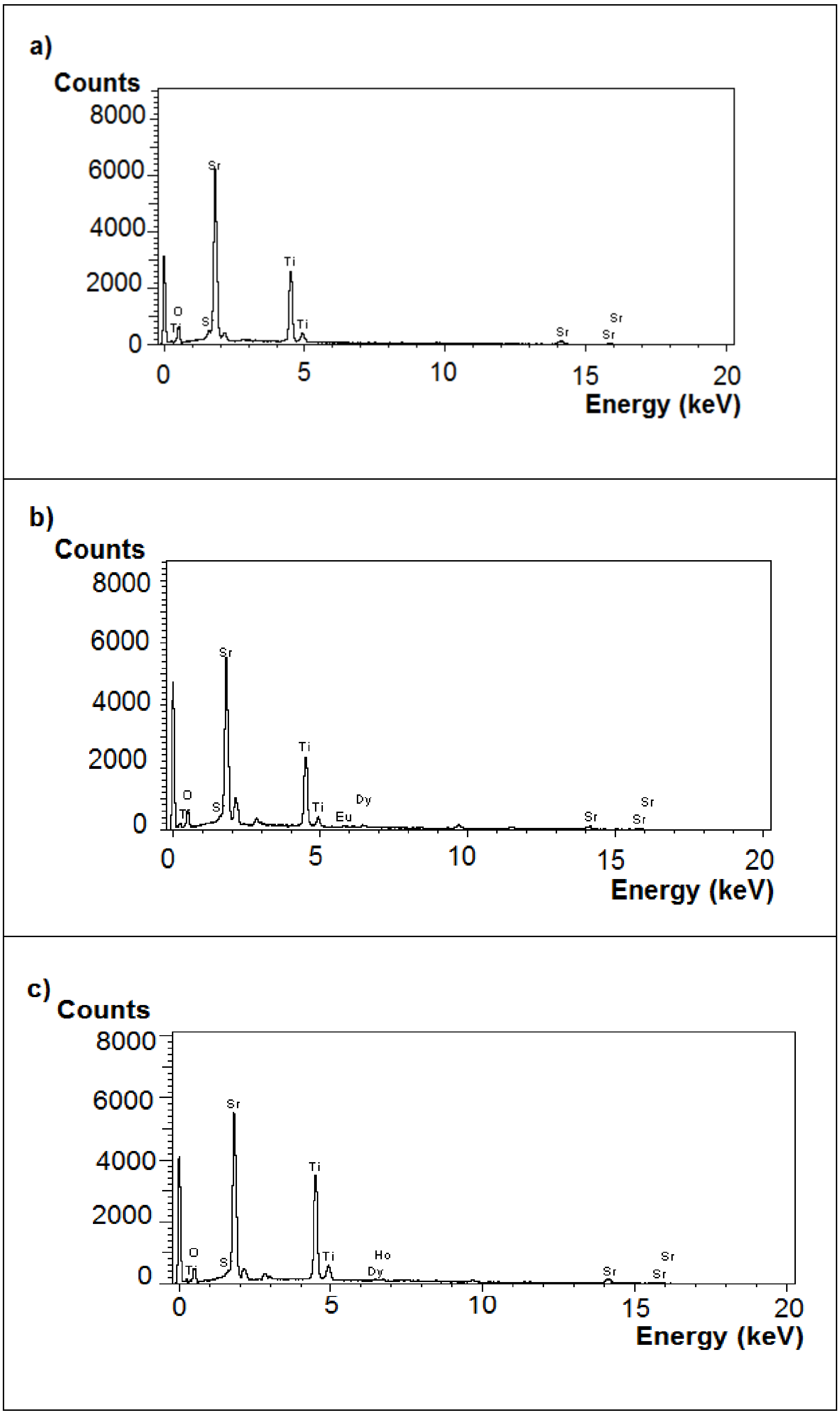

Fig.12. EDX analysis of (a) $SrTiO_3$, (b) $SrTiO_3$: Eu^{3+}(1% mol), Dy^{3+}(1% mol) and (c) $SrTiO_3$: Ho^{3+} (1% mol), Dy^{3+}(1% mol) samples.

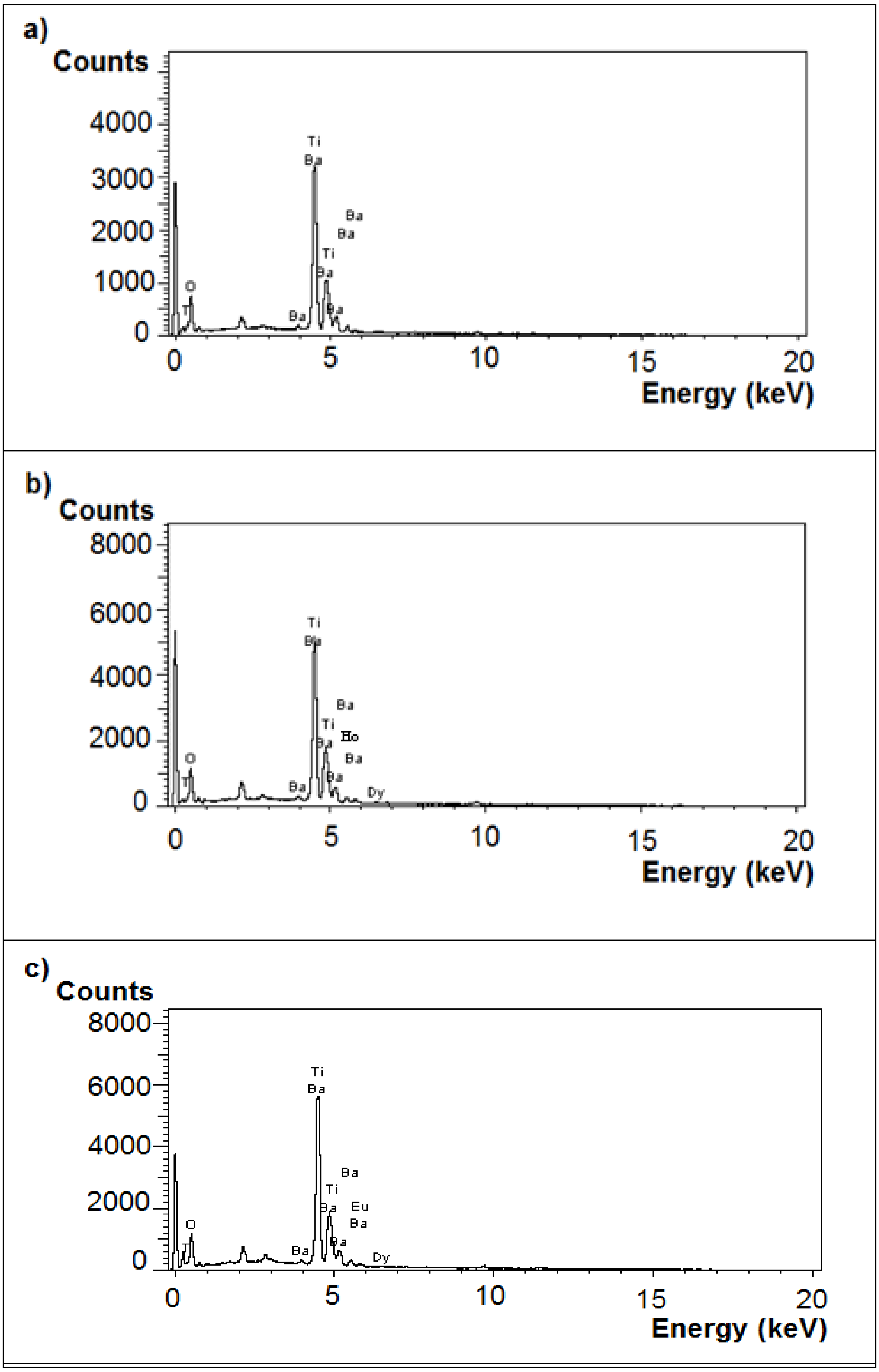

Fig.13. EDX analysis of (a) $BaTiO_3$, (b) $BaTiO_3$: Dy^{3+}(1% mol), Ho^{3+}(1% mol) and (c) $BaTiO_3$:Dy^{3+}(1% mol), Eu^{3+} (1% mol) samples.

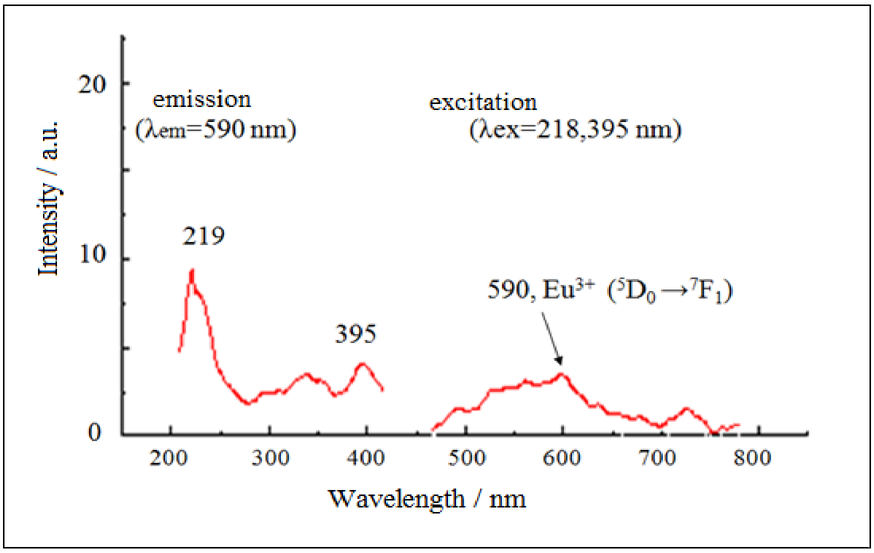

Fig. 14. Excitation and emission spectrum of Eu^{3+} (1% mol), Dy^{3+}(1% mol) doped $CaTiO_3$ system

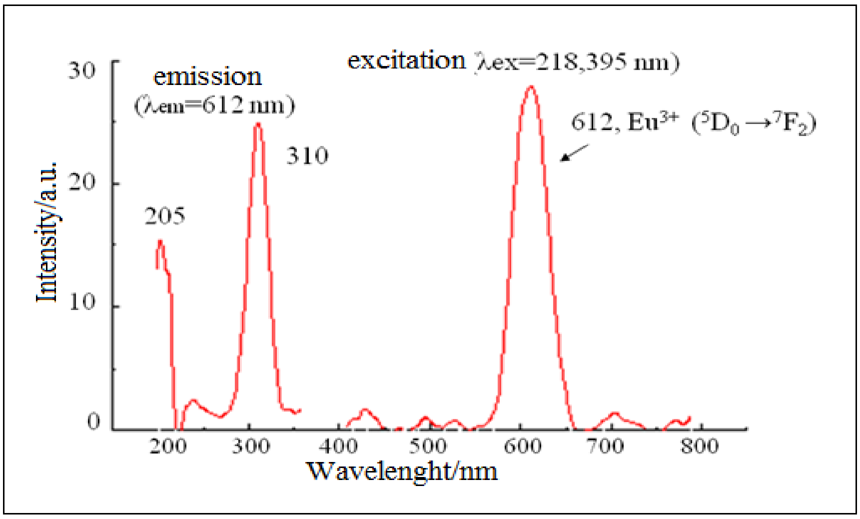

Fig. 15. Excitation and emission spectrum of Eu^{3+} (1% mol), Dy^{3+} (1% mol) doped $SrTiO_3$ system.

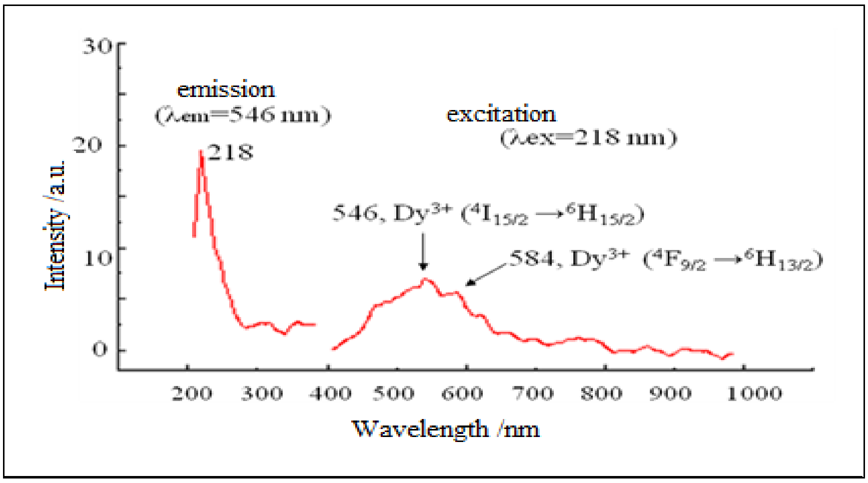

Fig.16. Excitation and emission spectrum of Dy^{3+} (1% mol), Ho^{3+}(1% mol) doped $BaTiO_3$ system.

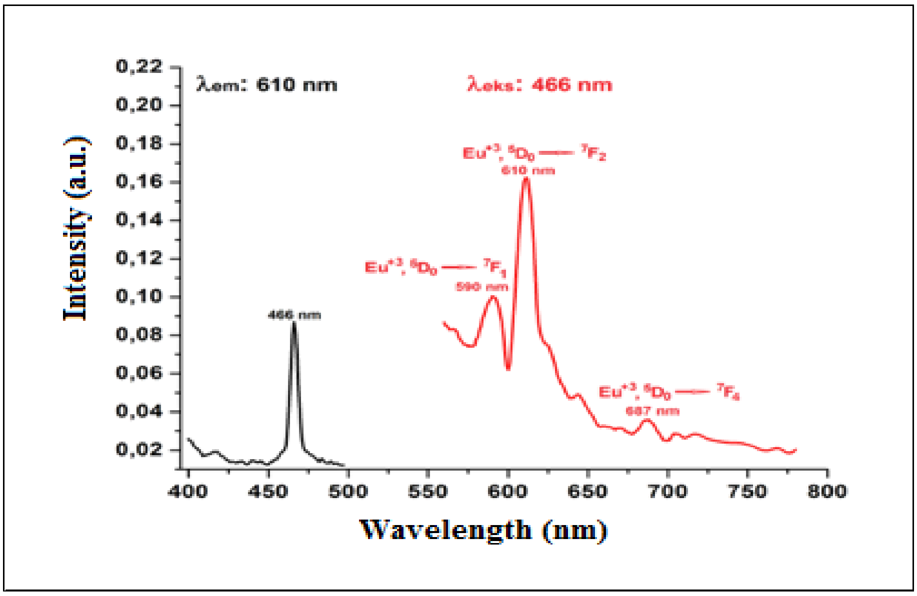

Fig.17. Excitation and emission spectrum of Dy^{3+} (1% mol), Eu^{3+}(1% mol) doped $BaTiO_3$

Table 2. XRD powder pattern data of $CaTiO_3$

No	h	k	l	2Θ$_{obs}$	2Θ$_{cal}$	d$_{obs(pm)}$	d$_{cal(pm)}$	I/I$_o$
1	0	1	1	23.23	23.23	382.54	382.51	12.8
2	1	1	1	26.03	26.03	342.06	342.05	3.6
3	2	1	1	33.11	33.11	270.31	270.31	100.0
4	0	2	1	37.06	37,00	242.40	242.77	2.3
5	1	2	1	38.89	38.89	231.39	231.38	8.5
6	2	2	0	40.68	40.68	221.62	221.62	6.5
7	3	1	1	42.61	42.61	211.99	212.00	2.6
8	2	2	1	44.16	44.16	204.91	204.91	3.7
9	0	2	2	47.50	47.50	191.27	191.26	57.0
10	3	2	0	48.95	48.95	185.93	185.94	6.0
11	0	3	1	53.25	53.25	171.88	171.87	4.6
12	1	3	1	54.69	54.69	167.69	167.68	6.1
13	2	3	1	58.87	58.87	156.75	156.74	19.9
14	4	2	2	69.49	69.49	135.15	135.15	13.0
15	2	3	3	79.12	79.12	120.95	120.95	7.9
16	4	4	0	88.08	88.08	110.81	110.81	3.3

Table 3. XRD powder pattern data of $CaTiO_3$: Eu^{3+} (1% mol), Dy^{3+}(1% mol)

No	h	k	l	2Θ$_{obs}$	2Θ$_{calc}$	d$_{obs\ (pm)}$	d$_{calc(pm)}$	I/I$_o$
1	0	1	1	23.23	23.23	382.54	382.51	12.8
2	1	1	1	26.03	26.03	342.06	342.05	3.6
3	2	1	1	33.11	33.11	270.31	270.31	100.0
4	0	2	1	37.06	37,00	242.40	242.77	2.3
5	1	2	1	38.89	38.89	231.39	231.38	8.5
6	2	2	0	40.68	40.68	221.62	221.62	6.5
7	3	1	1	42.61	42.61	211.99	212.00	2.6
8	2	2	1	44.16	44.16	204.91	204.791	3.7
9	0	2	2	47.50	47.50	191.27	191.26	57.0
10	3	2	0	48.95	48.95	185.93	185.94	6.0
11	0	3	1	53.25	53.25	171.88	171.87	4.6
12	1	3	1	54.69	54.69	167.69	167.68	6.1

Table 4. Unit cell parameters of $SrTiO_3$, $SrTiO_3$: Eu^{3+} (1% mol), Dy^{3+}(1% mol) and $SrTiO_3$: Ho^{3+} (1% mol), Dy^{3+}(1% mol)

Sample	a/pm	V/pm^3
$SrTiO_3$	390.50	596.00 10^5
$SrTiO_3$: Eu^{3+}(1%),Dy^{3+}(1%),	390.49	535.44.10^5
$SrTiO_3$: Ho^{3+}(1%),Dy^{3+}(1%),	390.51	595.50.10^5

Table 5. XRD powder pattern data of $SrTiO_3$

No	h	k	l	$2\Theta_{obs}$	$2\Theta_{calc}$	d_{obs} (pm)	d_{calc} (pm)	I/I$_o$
1	1	0	0	22.75	22.75	390.51	390.51	3.3
2	1	1	0	32.40	32.40	276.13	276.13	100
3	1	1	1	39.96	39.96	225.46	225.46	20.8
4	2	0	0	46.47	46.47	195.25	195.25	39.7
5	2	1	1	57.79	57.79	159.42	159.42	32.9
6	2	2	0	67.82	67.82	138.07	138.07	18.8
7	3	1	0	77.18	77.18	123.49	123.49	10.3
8	3	1	1	81.72	81.72	117.74	117.74	3.5
9	2	2	2	86.21	86.21	112.73	112.73	4.5

Table 6. XRD powder pattern data of $SrTiO_3$: Eu^{3+} (1% mol), Dy^{3+}(1% mol)

No	h	k	l	$2\Theta_{obs}$	$2\Theta_{calc}$	d_{obs} (pm)	d_{calc} (pm)	I/I$_o$
1	1	0	0	22.785	22.754	389.96	390.49	3.7
2	1	1	0	32.414	32.398	275.99	276.12	100
3	1	1	1	39.366	39.957	225.41	225.45	17.2
4	2	0	0	46.498	46.473	195.15	195.25	37.6
5	2	1	1	57.784	57.789	159.43	159.42	26.7
6	2	2	0	67.820	67.828	138.06	138.06	14.6
7	3	1	0	77.187	77.189	123.49	123.49	9.5
8	3	1	1	81.724	81.725	117.74	117.74	2.9
9	2	2	2	86.205	86.211	112.73	112.73	3.4

Table 7. XRD powder pattern data of $SrTiO_3$: Ho^{3+}(1% mol), Dy^{3+}(1% mol)

No	h	k	l	$2\Theta_{obs}$	$2\Theta_{calc}$	d_{obs} (pm)	d_{calc}(pm)	I/I$_o$
1	1	0	0	22,751	22,753	390,55	390,51	4,5
2	1	1	0	32,396	32,397	276,13	276,13	100,0
3	1	1	1	39,955	39,956	225,47	225,46	23,7
4	2	0	0	46,471	46,471	195,25	195,25	32,3
5	2	1	1	57,783	57,786	159,43	159,42	29,7
6	2	2	0	67,821	67,825	138,07	138,06	18,4
7	3	1	0	77,184	77,186	123,49	123,49	9,1
8	3	1	1	81,724	81,722	117,74	117,74	3,8
9	2	2	2	86,210	86,207	112,73	112,73	5,4

Table 8. Unit cell parameters of $BaTiO_3$, $BaTiO_3$:Dy^{3+} (1% mol), Ho^{3+}(1% mol) and $BaTiO_3$: Dy^{3+}(1% mol), Eu^{3+}(1% mol)

Sample	a-b/pm	c/pm	V/pm^3
$BaTiO_3$	400.90	400.28	643.00.10^5
$BaTiO_3$: Dy^{3+}(1%), Ho^{3+}(1%)	400.92	400.27	633.38.10^5
$BaTiO_3$: Dy^{3+}(1%), Eu^{3+}(1%)	400.91	400.28	643.36.10^5

Table 9. XRD powder pattern data of $BaTiO_3$

No	h	k	l	$2\Theta_{obs}$	$2\Theta_{calc}$	d_{obs} (pm)	d_{calc} (pm)	I/I_o
1	0	0	1	22.190	22.190	400.28	400.28	17.1
2	1	1	0	31.535	31.535	283.48	283.48	100.0
3	1	1	1	38.899	38.899	231.34	231.34	29.2
4	0	0	2	45.273	45.273	200.14	200.14	17.9
5	1	0	2	50.956	50.957	179.07	179.07	7.1
6	1	1	2	56.215	56.216	163.50	163.50	22.9
7	2	0	2	65.897	65.897	141.63	141.63	10.2
8	0	0	3	70.523	70.524	133.43	133.43	2.9
9	1	0	3	74.955	74.956	126.60	126.60	9.3
10	1	1	3	79.299	79.296	120.72	120.72	3.1
11	2	2	2	83.510	83.510	115.67	115.67	7.2

Table 10. XRD powder pattern data of $BaTiO_3$: Dy^{3+} (1% mol), Ho^{3+}(1% mol)

No	h	k	l	$2\Theta_{obs}$	$2\Theta_{calc}$	d_{obs} (pm)	d_{calc} (pm)	I/I_o
1	0	0	1	22.19	22.19	400.33	400.27	14.9
2	1	1	0	31.50	31.53	283.78	283.49	100.0
3	1	1	1	38.87	38.89	231.49	231.35	42.4
4	0	0	2	45.27	45.27	200.15	200.13	18.8
5	1	0	2	50.96	50.96	179.07	179.6	6.3
6	1	1	2	56.22	56.22	163.50	163.50	28.2
7	2	0	2	65.90	65.90	141.63	141.63	12.7
8	0	0	3	70.53	70.53	133.43	133.42	5.5
9	1	0	3	74.96	74.96	126.59	126.60	6.6
10	1	1	3	79.30	79.30	120.72	120.72	4.0
11	2	2	2	83.51	83.51	115.67	115.67	7.3

Table 11. XRD powder pattern data of $BaTiO_3$: Dy^{3+} (1% mol), Eu^{3+} (1% mol)

No	h	k	l	$2\Theta_{obs}$	$2\Theta_{calc}$	d_{obs} (pm)	d_{calc} (pm)	I/I_o
1	0	0	1	22.19	22.19	400.21	400.28	13.7
2	1	1	0	31.54	31.53	283.47	283.49	100.0
3	1	1	1	38.90	38.90	231.33	231.34	27.9
4	0	0	2	45.27	45.27	200.13	200.14	26.0
5	1	0	2	50.96	50.96	179.06	179.07	9.4
6	1	1	2	56.21	56.22	163.50	163.50	23.1
7	2	0	2	65.89	65.90	141.63	141.63	17.2
8	0	0	3	70.52	70.52	133.43	133.43	4.5
9	1	0	3	74.96	74.96	126.60	126.60	9.2
10	1	1	3	79.30	79.30	120.72	120.72	6.2
11	2	2	2	83.51	83.51	115.67	115.67	6.5

Table 12. The elemental analysis of $CaTiO_3$ and $CaTiO_3$: Eu^{3+}(1% mol), Dy^{3+}(1% mol), $SrTiO_3$, $SrTiO_3$: Eu^{3+} (1% mol), Dy^{3+}(1% mol), $SrTiO_3$:Ho^{3+}(1% mol), Dy^{3+}(1% mol), $BaTiO_3$, $BaTiO_3$: Dy^{3+}(1% mol), Ho^{3+}(1% mol), and $BaTiO_3$: Dy^{3+}(1% mol), Eu^{3+}(1% mol) data

	Calculated				**Experimental**			
	Ca	Ti	O	Lanthanum series elements	Ca	Ti	O	Lanthanum series elements
$CaTiO_3$	29.48	35.22	35.30	--	29.54	33.19	37.27	--
$CaTiO_3$: Eu^{3+}(1% mol), Dy^{3+}(1% mol)	26.34	31.46	31.52	10.68	28.01	29.10	33.11	9.77
	Sr	Ti	O	Lanthanum series elements	Sr	Ti	O	Lanthanum series elements
$SrTiO_3$	47.75	26.09	26.16	--	49.85	24.24	25.91	--
$SrTiO_3$: Eu^{3+}(1% mol), Dy^{3+}(1% mol)	47.75	26.09	26.16	1.69	49.12	22.95	25.61	1.24
$SrTiO_3$:Ho^{3+}(1% mol), Dy^{3+}(1% mol)	47.75	26.09	26.16	1.69	45.85	26.20	25.41	1.68
	Ba	Ti	O	Lanthanum series elements	Ba	Ti	O	Lanthanum series elements
$BaTiO_3$	58.88	20.53	20.60	--	58.34	20.18	21.48	--
$BaTiO_3$: Dy^{3+}(1% mol), Ho^{3+}(1% mol)	58.22	20.53	20.58	1.33	58.87	20.80	18.96	1.36
$BaTiO_3$: Dy^{3+}(1% mol), Eu^{3+}(1% mol)	58.22	20.53	20.58	1.332	56.83	20.28	20.91	1.62

Table 13. The color of samples under UV lamp excitation with 240 nm and 360 nm

Substances Synthesized	**Emission (nm)**	**Color under UV light** 240 nm (360 nm)	**Color in daylight**
$CaTiO_3$	517	Light yellow	Light yellow
$CaTiO_3$: Dy^{3+}(1%), Eu^{3+}(1%)	590	Yellow	Light yellow
$SrTiO_3$	559	Yellow (Red)	White
$SrTiO_3$:Dy^{3+}(1%), Eu^{3+}(1%)	612	Yellow	White
$SrTiO_3$: Dy^{3+}(1%), Ho^{3+}(1%)	-	Dark yellow (Purple)	Light yellow
$BaTiO_3$	567	Yellow (pink)	Cream
$BaTiO_3$: Dy^{3+}(1%), Eu^{3+}(1%)	590-610	Dark Brown (Purple)	Cream
$BaTiO_3$: Dy^{3+}(1%), Ho^{3+}(1%)	546-584	Brown	Light Yellow

4. Conclusion

$CaTiO_3$, $SrTiO_3$ and $BaTiO_3$ host crystals were synthesized and doped with Dy^{3+}, Eu^{3+} and Ho^{3+} ions. Orthorhombic crystal system of $CaTiO_3$, cubic crystal system of $SrTiO_3$ tetragonal and crystal system of $BaTiO_3$ were determined in parallel agreement with the literature.

Doping Dy^{3+}, Eu^{3+} and Ho^{3+} ions does not change unit cell parameters of host crystals. The characteristic emission peaks of Dy^{3+}, Eu^{3+} and Ho^{3+} ions were determined.

Under UV lamp excitation with 240 nm and 360 nm, color of samples are listed in Table 13.

Acknowledgement

We acknowledge the financial support granted by Erciyes University (ERUBAP), FBY-12-3945 and ID: 3945.

References

[1] W.J. Jaffe, R. Cook, H. Jaffe, "Piezoelectric ceramics", Academic Press, New York (1971).

[2] M.E. Lines, A.M. Glass, "Principles and applications of ferroelectrics and related materials", Oxford University Press, Oxford (2001).

[3] J.F. Scott, "Applications of modern ferroelectrics", Science, 315 954–63 (2007).

[4] Y. Yang, X.H. Wang, C.K. Sun, L.T. Li, "Photoluminescence of high aspect-ratio $PbTiO_3$ nanotube arrays", J. Am. Ceram. Soc., 91 3820–2 (2008).

[5] G. Nenartaviciene, K. Tonsuaadu, D. Jasaitis, A. Beganskiene, A.Kareiva, "Preparation and characterization of superconducting $YBa_2(Cu_{1-x}Cr_x)_4O_8$ oxides by thermal analysis", J. Therm. Anal. Calorim., 90 173–81 (2007).

[6] M. Roy, P. Dave, S.K. Barbar, S. Jangid, D.M. Phase, AM. Awasth, "X-ray, SEM, and DSC studies of ferroelectric $Pb_{1-x}Ba_xTiO_3$ ceramics", J. Therm. Anal. Calorim., 101 833–40 (2010).

[7] A. Caneiro, L. Mogni, N. Grunbaum, F. Prado, "Physicochemical properties of non-stoichiometric oxides mixed conductors: part I", J. Therm. Anal. Calorim., 103 597–606 (2011).

[8] M.L. Moreira, M.F.C. Gurgel, G.P. Mambrini, E.R. Leite, P.S. Pizani, J.A. Varela, E. Longo "Photoluminescence of barium titanate and barium zirconate in multilayer disordered thin films at room temperature", J. Phys. Chem. A, 112 8938-8942 (2008).

[9] K.M. Lina, C.C. Lina, C.Y. Hsiaob, Y.Y. Lia, "Synthesis of $Gd_2Ti_2O_7$:Eu^{3+}, V^{4+} phosphors by sol–gel process and its luminescent properties", J. Lumin, 127 561-567 (2007).

[10] G.F.G. Freitas, R.S. Nasar, M. Cerqueira, D.M.A. Melo, E. Longo, J.A. Varel, "Luminescence in semi-crystalline zirconium titanate doped with lanthanum", Mater. Sci. Eng. A., 434 19-22 (2006).

[11] I. Wuled Lenggoro, C. Panatarani, K. Okuyama, "One-step synthesis and photoluminescence of doped strontium titanate particles with controlled morphology", Mater. Sci.Eng. B. 113 60-66 (2004).

[12] J.K. Park, H. Ryu, H.D. Park, S.Y. Choi, "Synthesis of $SrTiO_3$:Al, Pr phosphors from a complex precursor polymer and their luminescent properties", J Eur Ceram Soc., 21 535-543 (2001).

[13] L. Hu, H. Song, G. Pan, B. Yan, R. Qin, Q.Dai, "Enhancement of red spectral emission intensity of $Y_3Al_5O_{12}$:Ce^{3+} phosphor via Pr co-doping and Tb substitution for the application to white LEDs", J. Lumin. 127 371-376 (2007).

[14] A. Sinha, S.R. Nair, P.K. Sinha, "Single step synthesis of Li_2TiO_3 powder", J. Nucl. Mater. 399 162-167 (2010).

[15] A.T. De Figueiredo, V.M. Longo, S. De Lazaro, V.R. Mastelaro, F.S. De Vicente, A.C. Hernandes, M. Li Siu, J.A. Varela, E. Longo, Blue-green and red photoluminescence in $CaTiO_3$:Sm, Journal of Luminescence. 126, 403–407, (2007).

[16] Katsumata, T., Kohno, Y., Kubo, H., Komuro S., Morikawa T., "Low temperature fluorescence thermometer application of long afterglow phosphorescent $SrAl_{12}O_{19}$: Eu^{2+},Dy^{3+} crystals", Revıew Of Scientific Instruments, 76, 8, (2005).